IL NUOVO CIMENTO VOL. 21 C, N. 6 Novembre-Dicembre 1998

Imaging spectroscopy in the visible near infrared of the Aristarchus region on the Moon

G. BELLUCCI, V. FORMISANO and S. PINORI

CNR, Istituto di Fisica dello Spazio Interplanetario - Via Fosso del Cavaliere, 00133 Roma, Italy

(ricevuto il 3 Marzo 1998; approvato il 15 Settembre 1998)

Summary. — In this paper we present a study of the Aristarchus region on the Moon by means of imaging spectroscopy data. We report the albedo, the UVVIS continuum and 0.9–1 μm absorption band maps, showing the complex pattern of Aristarchus crater ejecta and the distribution of surrounding materials. The extension of the dark mantling deposits present on Aristarchus plateau is well shown from our data, appearing very red and with a uniform distribution of the 0.9–1 μm band. By using principal component analysis and clustering techniques we have identified seven different spectral regions. The plateau is composed of two distinct spectral units, while Aristarchus and its ejecta blanket show a complex distribution of both feldspatic and basaltic materials.

PACS 95.55 – Astronomical and space-research instrumentation.
PACS 95.75 – Observation and data reduction techniques; computer modeling and simulation.
PACS 96.20.Dt – Features, landmarks, mineralogy, petrology and atmosphere.
PACS 95.75.Fg – Spectroscopy and spectrophotometry.

1. – Introduction

Traditional techniques as multiband imaging and spot spectroscopy, have been extensively used in the past for the study of the Moon. Imaging spectroscopy is a new technique which allows the spectral mapping of soils and identification of minerals making up the surface remotely sensed by using the spectrum of each pixel in the scene. From ground-based observatories, the Moon offers the unique possibility to have high-spatial-resolution image cubes that allow the study of different mineralogic units present on its surface. Although the unique identification of mafic minerals requires high-resolution spectra to 2.5 μm [1,2], UVVIS spectroscopy allows to obtain quantitative clues concerning glass and agglutinate content, TiO_2 content, ilmenite content and pyroxene composition [3,4]. The Aristarchus region is geologically and compositionally very complex and has been studied by lunar scientists since long time. It is dominated by the Aristarchus Plateau, an elevated

crustal block mainly composed of dark mantling deposits (DMD). This region presents a variety of spectral, radar and thermal peculiarities, including low albedo, lowest 3.8 cm and 70 cm radar reflectivity and low eclipse temperature [5, 6]. It has been also the subject of numerous spectroscopic investigations. Lucey [7] found in the Aristarchus crater three highlands assemblages, probable indication of the presence of a plutonic complex. The spectral data are compatible with the presence of olivine, gabbro, dunite and troctolite. These data also indicate that the Aristarchus impact fully penetrated the mare, exposing the underlying highland material. McEwen [8], using the Clementine data, has found in the central peak of the Aristarchus crater olivine-rich materials and outcrops of anorthosite, possible remnants of the ferroan anorthosite crust that formed in the early stage of the lunar history. In the following, we present UVVIS continuum slope, 0.9–1 μm absorption band and spectral maps (spatial resolution of 5 km/pixel and 96 spectral bands from 0.4 to 1.1 μm with $\Delta\lambda = 7.5$ nm) of the Aristarchus-Harbinger region that can be directly linked to the mineralogic composition using previous spectroscopic observations of the same region [7, 9-11].

2. – Observations and data reduction

The data have been obtained by using an imaging spectrometer in the 0.4–1.1 μm spectral range. The observations were carried out on July 22, 1994 at the Sierra Nevada Observatory, Granada (Spain), with a 1.5 m aperture telescope configured at f/8, giving a scale of 0.4 arcsec per pixel. The spectrometer used a Thomson CCD detector, 384 × 288 pixels of 23 × 23 μm dimensions and cooled by liquid nitrogen at −40° C. The light entering the spectrometer slit was focused and dispersed by a holographic grating mirror on the CCD, with the dispersion direction along the columns and the slit along the rows. This translates to a field of view of 384 × 0.4 = 154 arcsec along slit. The images were ob-

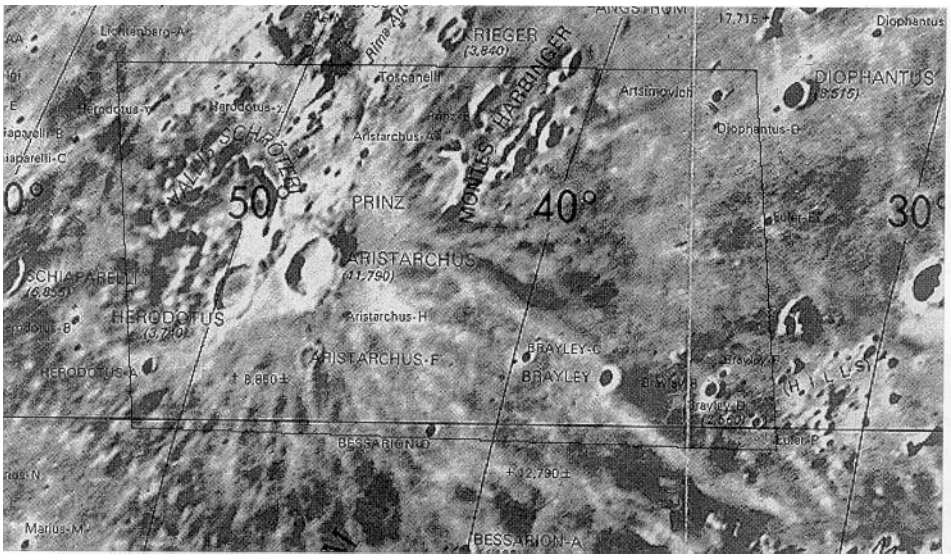

Fig. 1. – Map of the study region showing major features discussed in the text. The base map is by courtesy of Rand McNally & Company (1980).

tained by scanning the telescope across the lunar surface and acquiring each CCD frame during the motion. These frames were then packed into a tridimensional data set, called image cube. The readout electronics allowed the selection of different instrumental operation modes, by summing pixels on chip. We decided to sum 3 pixels spatially and 3 spectrally in order to increase the signal-to-noise ratio. This gave a theoretical spatial resolution of about 2.3 km and 96 spectral points of 7.5 nm bandwidth. However, after the data reduction and correction of various instrumental effects, the spatial resolution was degraded to about 3 km/pixel. Dark and flat field frames were acquired and the cubes corrected following standard techniques. The spectrometer was spectrally calibrated by means of measurements with monochromatic light before and after the observations. We have also acquired spectra of Jupiter and Saturn atmospheres that exhibit diagnostic methane bands and can be used as wavelength reference. The image cube was also corrected for the spectra curvature caused by the atmospheric refraction of light. Further details on the instrument and data reduction techniques can be found in [12]. Raw data were converted to relative spectral reflectance by rationing the raw spectrum of each pixel in the image by an average raw spectrum of the Mare Serenitatis 2 standard area (MS2 18° 40′ N 21° 25′ E [13]) which was acquired immediately after the Aristarchus image. Due to the high albedo of Aristarchus, the spectra of this crater were saturated in the 0.57–0.77 μm spectral range. The maps we report here have not been corrected for the geometrical distortion caused by the scanning process; the reader can refer to fig. 1 for the recognition of the main geological units present in the images that will be discussed in the following.

3. – Spectral properties of the studied region: albedo and band ratios

From 0.4–1.1μm spectroscopy of lunar soils three reflectance properties can be measured: the albedo, the UVVIS slope and the 0.9–1μm absorption band depth. Using these three quantities it is possible to infer about the mineralogy of the region under study [3,4,14]. For instance, plagioclase feldspate and low mafic minerals exhibit relatively high brightness, while mafic materials, like basalts, are darker and have a strong absorption band near 1 μm. The character of this band is affected also by the soil maturity. The UVVIS slope depends upon both the composition and maturity of the soils. The highlands exhibit generally a steeper slope than the maria. The position of the 0.9–1 μm band is also diagnostic of the mineralogic composition of the soils shifting toward longer wavelengths with the increasing content of Ca-pyroxene. We do not report a map of the 0.9–1 μm band position over all the image, because this would require a very accurate calibration of the spectra, a task which is not yet completed at the moment. In fig. 2, respectively, the albedo, the 0.9–1 μm absorption and the UVVIS slope maps are shown. The Aristarchus crater is very bright and this fact has caused the saturation of spectral channels from 0.57 to 0.77 μm. The UVVIS slope was computed by means of the 0.80/0.50 μm ratio while the depth of the 1 μm absorption has been determined through the 0.80/0.95 μm ratio. This quantity gives an estimate of the absorption because the true value can be found only by knowing the continuum at the band center and can be determined by using spectra up to 2.5 μm [15, 7]. In fig. 2 (center) bright tones indicate a greater abundance of iron-magnesium–rich materials; the absorption values span between 0.97 and 1.09. In fig. 2 (center) bright pixels represent "red" regions; the values of the slope span from 0.87 for dark pixels to 1.1 for the brighter regions. The dark mantling deposits (DMD) covering most of the plateau exhibit high UVVIS slopes; also a region around Montes Harbinger shows this red character; both these units have an absorption in the 0.9–1μm region lower

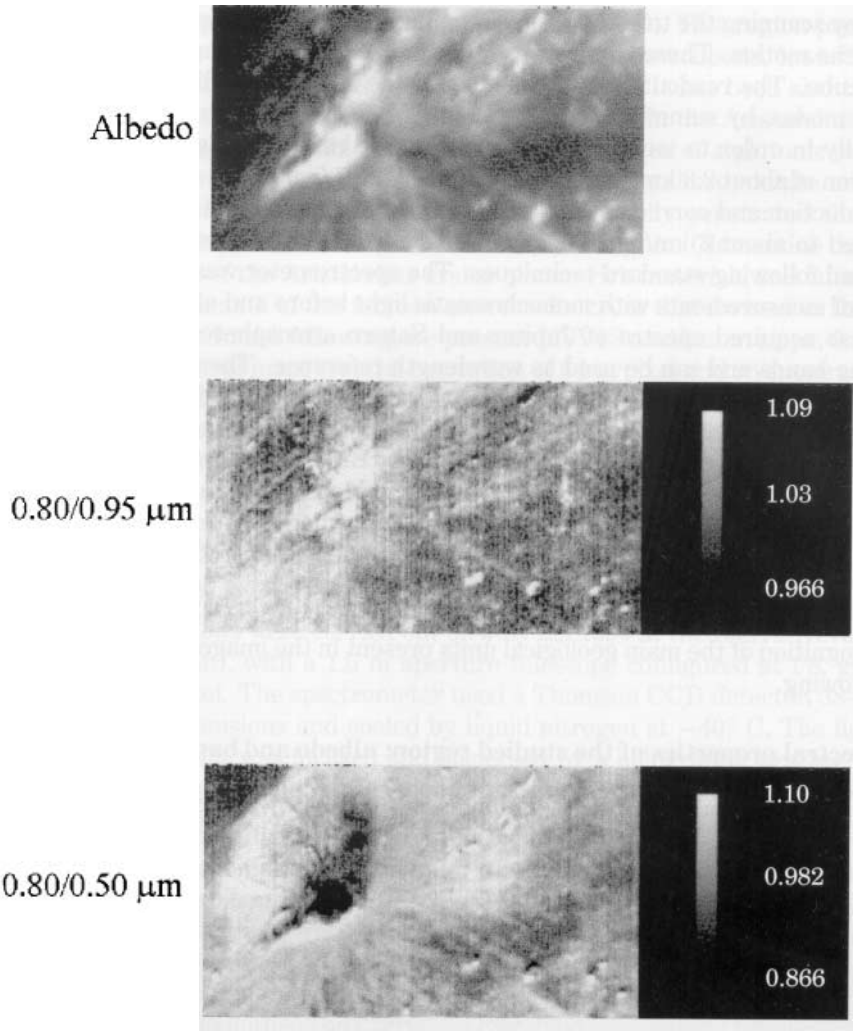

Fig. 2. – Albedo (top), 0.80/0.95 μm ratio image giving an estimation of the 0.9–1.1 μm absorption strength (center) and 0.80/0.50 μm ratio image proportional to the UVVIS slope (bottom).

than the Aristarchus ejecta extending to the north and some of the fresh craters visible in the image. The DMD show a homogeneous distribution of the 0.9–1μm absorption (fig. 2 (bottom)) with some contamination due to the Aristarchus and Aristarchus A ejecta. Most of the Aristarchus ejecta northward and westward the crater and Aristarchus A exhibit a flatter continuum. These values are computed with respect to a MS2 spectrum and 0.80/0.50 μm values less than one mean a negative slope of the soil with respect to Mare Serenitatis. This characteristic, together with the high albedo, is peculiar of feldspatic materials exposed at highland fresh craters [16, 14, 17]. While most of Aristarchus crater exhibits negative UVVIS slopes (0.80/0.50 μm $\approx$ 0.87), the 0.80/0.95 μm image shows a different distribution of the band depth across the crater. Two spots are visible inside the crater showing high 1 μm absorption (0.80/0.95 μm $\approx$ 1.05) while the rest of crater

exhibits a weaker absorption. Assuming the maturity of these soils to be the same, the difference in band depths mirrors the different abundance of mafic minerals. The albedo of this unit is very high; inside this crater feldspatic material with different abundance of mafic minerals can be present. The Aristarchus ejecta blanket is made of at least two different spectral units. The former includes the materials extending from northeast to northwest and covering part of Herodotus. Also the Aristarchus rim could be part of this class (it is difficult to judge due to the low spatial resolution). This spectral unit displays negative UVVIS slope and generally medium 1 μm absorption; a small region northward of Herodotus exhibits higher band depths. The second spectral unit is made of the materials present southward of Aristarchus and extending toward Herodotus. Its spectral peculiarities are high albedo, red slope and weak 1 μm absorption, characteristics of mature feldspatic soils. The materials extending northward of Aristarchus and southward of Aristarchus A could be of basaltic composition. In fact, they have an albedo lower than the surrounding fresh material and exhibit negative UVVIS slope and strong 1 μm absorption. The Aristarchus A ejecta blanket has spectral characteristics diagnostic of feldspatic composition (high albedo, negative UVVIS slope and deep 1 μm absorption). The absorption depth of the spectral units described above is controlled both by the physical status of the soils and by the mineralogic composition. For instance, a feldspatic breccia has a 1 μm absorption deeper than a mature highland soil. On the other hand, the band posi-

TABLE I. – *Principal component analysis statistics relative to the data sets discussed in the text.*

Full data set

PC Image	Image Min	Image Max	Image Mean	Image Stdev	Eigenvalue
1	0.0000	2.3694	0.9375	0.1587	2.2293
2	0.0000	2.3406	0.9430	0.1584	0.2104
3	0.0000	2.3525	0.9448	0.1603	0.0197
4	0.0000	2.3357	0.9458	0.1613	0.0081
5	0.0000	2.3357	0.9481	0.1601	0.0017
6	0.0000	2.3469	0.9470	0.1588	0.0011
7	0.0000	2.3180	0.9434	0.1568	0.0007
8	0.0000	2.3067	0.9445	0.1568	0.0003
9	0.0000	2.2997	0.9463	0.1562	0.0003
10	0.0000	2.2601	0.9420	0.1548	0.0002

Reduced data set

PC Image	Image Min	Image Max	Image Mean	Image Stdev	Eigenvalue
1	0.0000	2.3694	0.9375	0.1587	1.5569
2	0.0000	2.3406	0.9430	0.1584	0.2019
3	0.0000	2.3525	0.9448	0.1603	0.0148
4	0.0000	2.3357	0.9458	0.1613	0.0021
5	0.0000	2.3357	0.9481	0.1601	0.0009
6	0.0000	2.3469	0.9470	0.1588	0.0004
7	0.0000	2.3180	0.9434	0.1568	0.0003
8	0.0000	2.3067	0.9445	0.1568	0.0002
9	0.0000	2.2997	0.9463	0.1562	0.0002
10	0.0000	2.2601	0.9420	0.1548	0.0001

tion moves toward longer wavelengths with increasing amount of Ca-pyroxene and olivine content; this causes also changing in the band depth. From the maps shown in fig. 2, it is then not possible to discriminate between mafic and ultramafic composition and we must rely upon high-resolution spectra extending up to 2.5 μm. In a following section we will compare our results with those of Lucey *et al.* [7], Hawke *et al.* [9] and Pinet *et al.* [11] in order to better quantify the composition of this region.

4. – Principal Component Analysis

A common technique used to enhance the information content of multiband data is the Principal Component Analysis (PCA [18-22, 11]). It uses a linear transformation of the data to translate and rotate them in a new coordinate system that maximizes the variance. After this transformation, the new components are statistically independent and the information is contained in few PC images while most of the noise is segregated in the other components. Mathematically, the PCA involves the calculation of the eigenvectors of the variance-covariance matrix of the data and then the transformation of the data onto a set of orthogonal axes that are linear combination of the original data. The first transformed image normally depicts the average brightness of the surface while the other components contain the color information and are generally pairwise differences between the original spectral channels. As we have mentioned above, the pixels in the Aristarchus crater had spectra saturated in the 0.57–0.77 μm spectral region. In order to study also the crater, we have applied the PCA technique to the MS2 rationed image cube using the full data set (121 $\times$ 206 spectra; 94 bands) and a reduced one (121 $\times$ 206 spectra; 66 bands) having excluded from the latter the 27 saturated channels. From the analysis the last two channels were also excluded because they exhibited very noisy values (1.101 μm and 1.108 μm). In table I the relevant statistic for 10 components is reported. Both the eigenvalues and the PC images (eigenvectors) are used to evaluate the number of meaningful components. Eigenvalues for bands that contain information will be an order of magnitude larger than those that contain only noise. The corresponding images will be spatially coherent, while the noise images will not contain any spatial information. The meaningful components are, respectively, 7 for the full data set and 5 for the reduced one: the corresponding PC images are shown in fig. 3. We will indicate with PC_f the full data set and with PC_r the reduced data set of PC images. The comparison between the two sets of PC images shows that the 0.57–0.77 μm spectral range allows to better discriminate the dark mantling materials covering most of the plateau. They are well visible in the PC_{f7} image while are not on the PC_r maps. This demonstrates the great utility of imaging spectroscopy in the study of the Moon with respect to conventional multiband (less than 10 wavelengths) imaging. All the tremendous spectral variability of the Aristarchus region is visible from both the data sets. In some PC image, the spatial resolution has been improved (see, for example, PC_{f4}), allowing to recognize narrow features like Vallis Schroteri. The Aristarchus crater appears spectrally variegated. In the $PC_{r3,5}$ images, some circular features are visible inside the crater or close to the rim. This spectral variability has been also observed by [7] and [10, 11]. Lucey suggested that it is consistent with the presence of an excavated plutonic complex and the circular features observed in the 0.80/0.95 μm ratio and PC_r images could be the remnants of it. The Aristarchus ejecta extending southwest of the crater are visible in most of the PC images, while the complex pattern of materials toward the plateau and Aristarchus A is visible in few images, appearing sometimes as bright feature (PC_{f5}, PC_{r4}), sometimes dark (PC_{f3} and PC_{r3}).

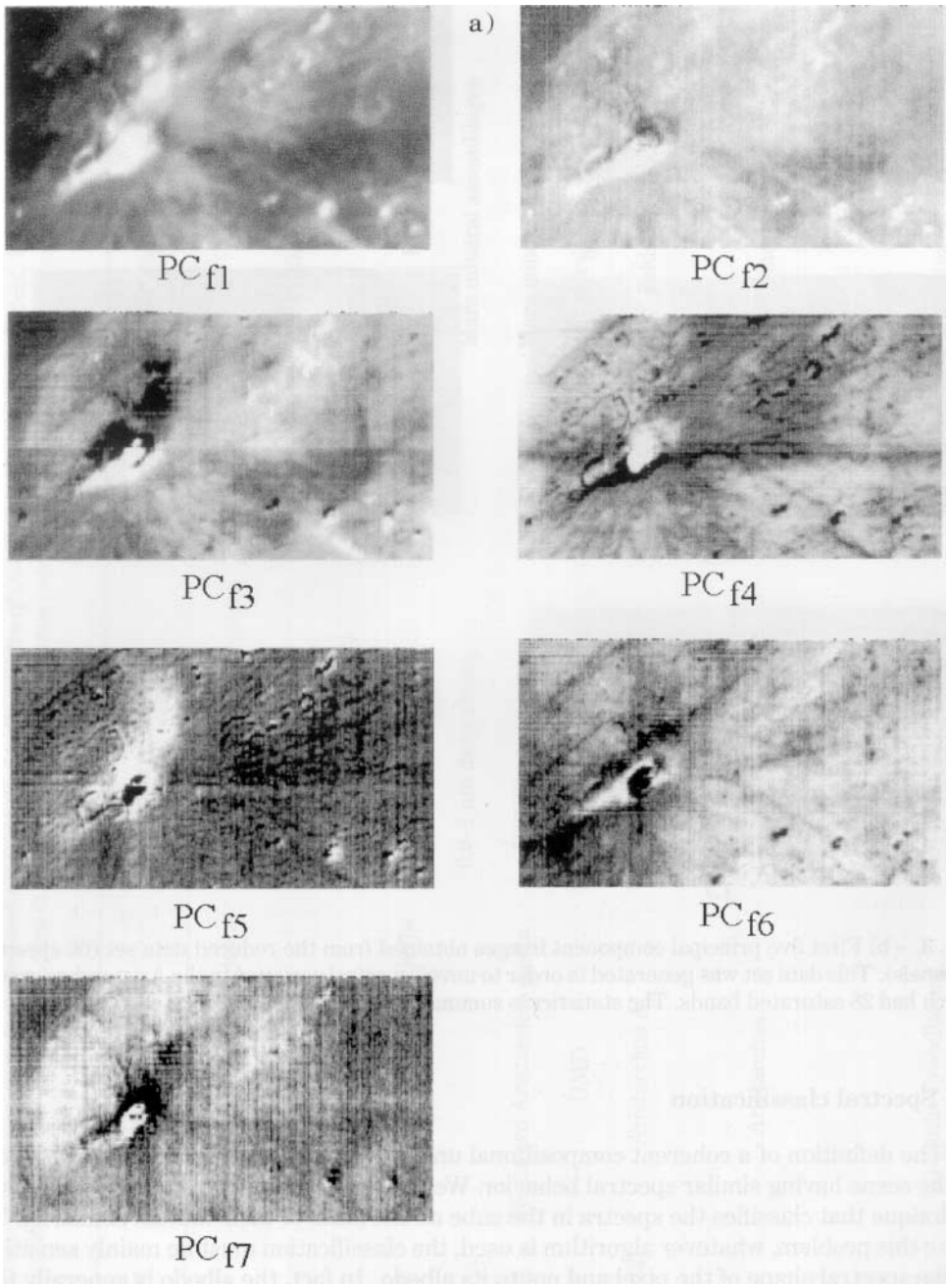

Fig. 3. – a) First seven principal component images obtained from the full data set (94 spectral channels). The statistics is summarized in table I.

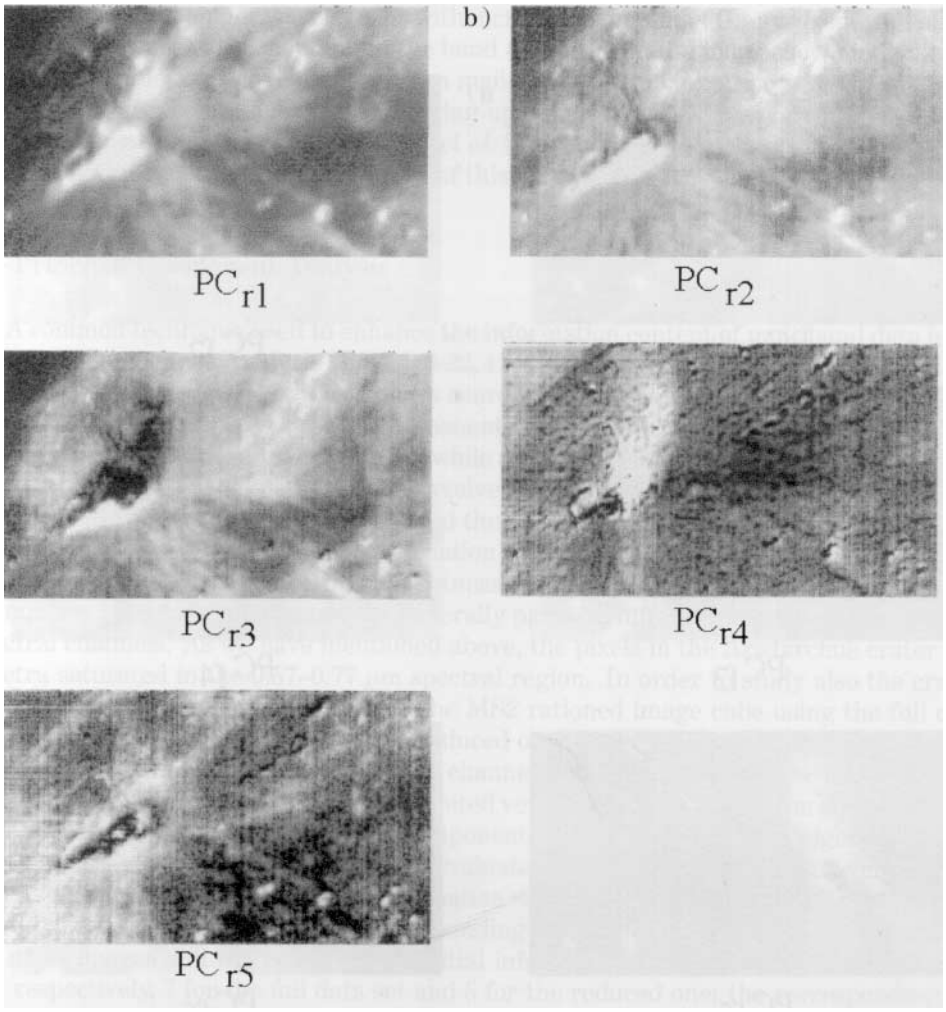

Fig. 3. – b) First five principal component images obtained from the reduced data set (66 spectral channels). This data set was generated in order to unveil spectral variation in the Aristarchus crater which had 28 saturated bands. The statistics is summarized in table I.

5. – Spectral classification

The definition of a coherent compositional unit requires the identification of all pixels in the scene having similar spectral behavior. We faced this problem by using a clustering technique that classifies the spectra in the cube on the basis of their mutual similarity. To solve this problem, whatever algorithm is used, the classification must be mainly sensitive to the spectral shape of the pixel and not to its albedo. In fact, the albedo is generally the major cause of difference in spectra of lunar soils and can easily mask the variation due to either the 1 μm absorption or the UVVIS slope. Nevertheless, the albedo is also a diagnostic parameter [4] which allows to distinguish bright feldspatic materials from dark basaltic soils and must be taken into account. We have then used an algorithm insensitive to albedo to find homogeneous spectral classes and used (*a posteriori*) the albedo to better qualify

TABLE II. – *Classes obtained through a clustering technique applied to the spectra of image cube discussed in the text. The mineralogic interpretation shown in the last column has been taken from Lucey et al.* [7]. *In italics, a tentative interpretation based on spectral analysis of our data is reported.*

Class	Color	Main regions	Spectral features	Class size (%)	Mineralogic interpretation
1	Red	Southward Aristarchus ejecta	Shallow UVVIS positive slope	2.2	*Olivine*
			1 μm absorption		*Mare mineral assemblages*
			Inflection at 0.65 μm		
2	Blue	Northward Aristarchus ejecta	UVVIS negative slope	0.82	Feldspar
			0.9–1 μm deep absorption		Mare mineral assemblages
3	Yellow	Westward Aristarchus ejecta	UVVIS negative slope	17.7	Mare mineral assemblages
4	Cyan	DMD	Shallow UVVIS positive slope	11	Fe^2 bearing glass
5	Magenta	Aristarchus A	Flat UVVIS slope	3	Feldspar, augite
			0.9–1.1 μm deep absorption		
6	Black	Aristarchus	UVVIS negative slope	0.1	Augite, olivine, probable feldspate
			0.9–1 μm deep absorption		
			Peak at 0.45 μm		
7	Purple	Oceanus Procellarum	Flat	61.8	*Mare mineral assemblages*

the compositional nature of the classes. The spectral classification has been done by using the spectral angle mapper classifier (SAM in the following [23,24]). SAM is an automated method for comparing image spectra to individual spectra. The algorithm determines the similarity between two spectra by calculating the angle α between them, treating them as vectors in a space with dimensions equal to the number of bands. The SAM algorithm is insensitive to the average brightness level of each spectrum (it uses the "direction" and not the "length" of the spectra); the spread inside each class with respect to the mean will be due only to spectral differences. SAM has been applied to the relative reflectance spectra; more details concerning this procedure are found in Bellucci and Formisano [25]. The use of SAM method requires the choice of training site spectra with respect to which to compute the angle values. Definition of training sites has been done on the basis of the PC images, the 0.80/0.50 μm and 0.80/0.95 μm ratios. The locations of training sites is shown in fig. 4a) while the classification map is shown in fig. 4b); it has been obtained by coloring the pixels having an α value less than 20×10^{-3} radians (the threshold has been fixed on the basis of instrumental noise). Each class has been colored by using the

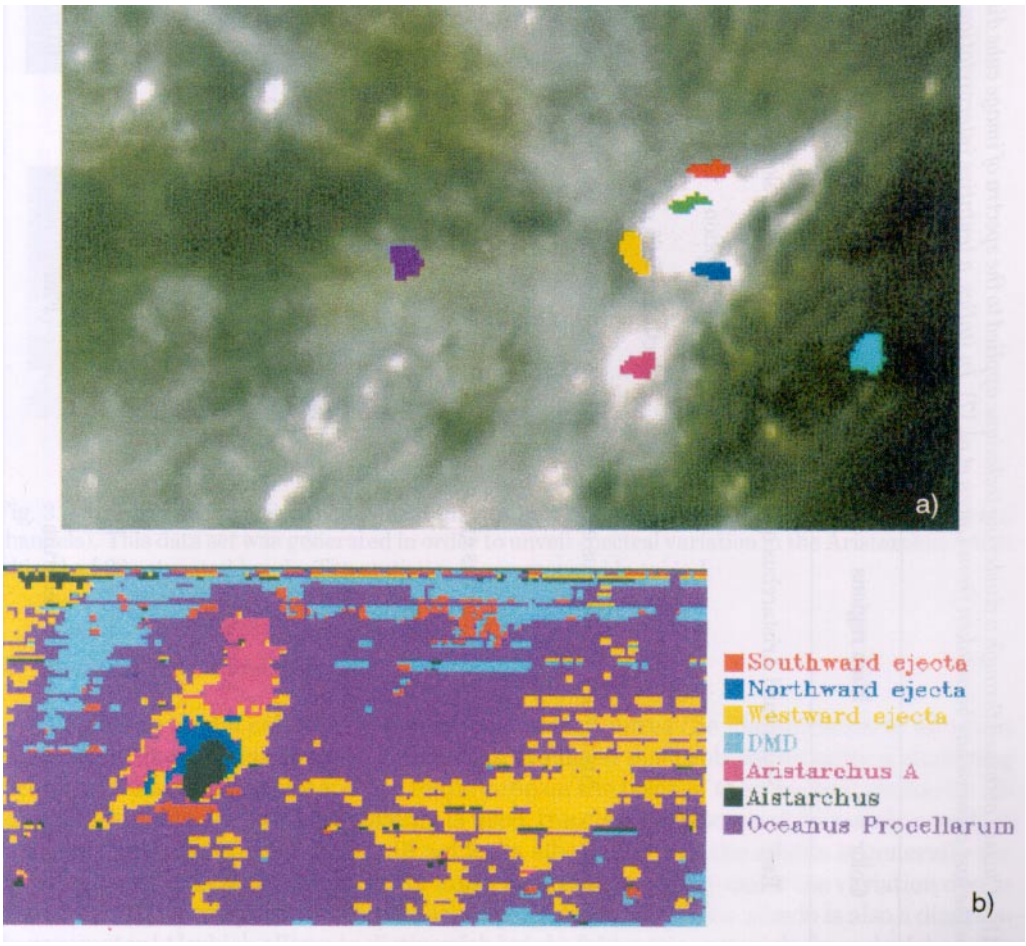

Fig. 4. – a) Training sites used to generate the classification map. Each color is used to identify the classes. b) Classification map obtained through the SAM algorithm (see the text).

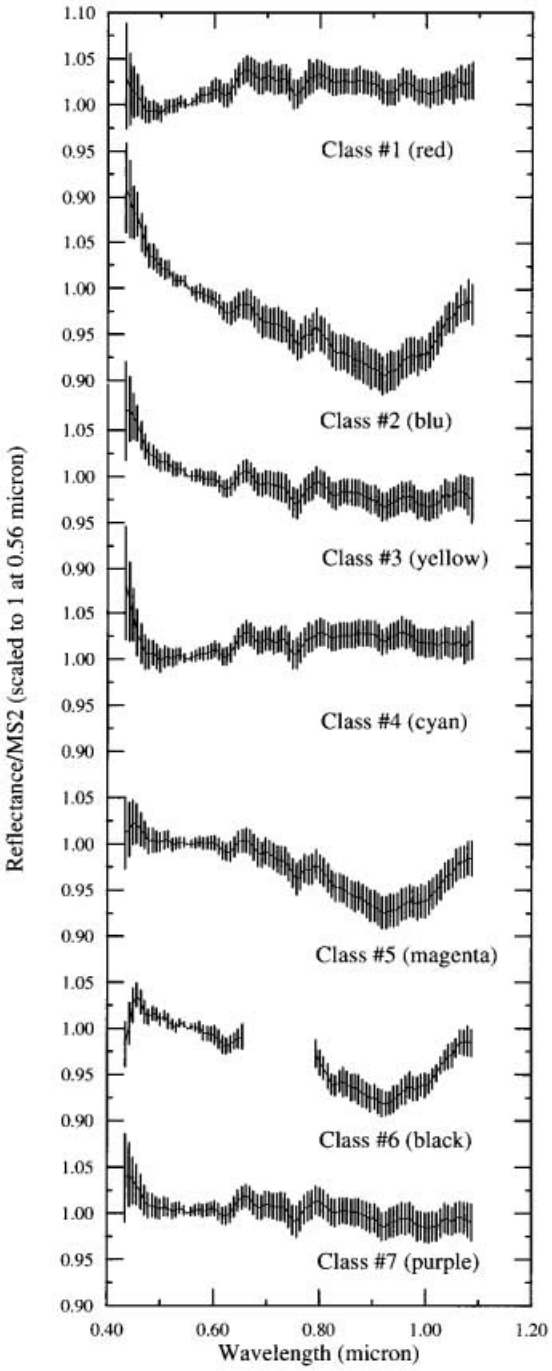

Fig. 5. – Spectra of the classes obtained by using the algorithm described in the text. The training classes have been chosen in the zones indicated in fig. 4a). The error bars indicate two standard deviations from the mean. The Aristarchus class had 28 spectral channels saturated which have been masked.

corresponding training site color. The average spectrum of the classes is shown in fig. 5 and their main characteristics are summarized in table II. It must be remembered that the spectra are relative to MS2 and their shape reflects the difference of each specific soil to that in Mare Serenitatis. The class #7 (purple) is the largest (61.8 % of the pixels) : it is spectrally flat, mirroring the fact that it is composed mainly of the Oceanus Procellarum basalts. The class #3 (yellow) is characterized by a shallow negative UVVIS slope and represents mainly the low-albedo materials present on Oceanus Procellarum, suggesting a TiO_2 content higher in these soils than in the most part of Oceanus Procellarum covered by our image. The same class, however, contains spectra of bright regions present in the Aristarchus ejecta blanket (see also fig. 4a)) which could be of feldspatic origin. The 1 μm absorption is comparable in strength with Mare Serenitatis basalts indicating the presence of fair amounts of pyroxene; if feldspate is present in the bright materials, it could have a composition dominated by clinopyroxene. Class #5 represents also two units having very different albedo values: Aristarchus A crater (and the surrounding ejecta blanket) and the materials northward of Herodotus. The spectra that belong to this class have a strong 1 μm absorption and flat UVVIS slope. The bright materials could be of feldspatic composition, while basalts dominate the mineralogic assemblages of darker soils. Aristarchus and its northward ejecta belong to classes very similar (classes #6 and #2). The corresponding spectra have strong negative UVVIS slope and strong 1 μm absorption. Notable differences between the classes are, however, the UVVIS slope and the presence in the Aristarchus class of an inflection at 0.45 μm. All the Aristarchus crater has been classified of one spectral type due to the saturation occurred in the 0.57–0.77 channels. Other spectral units can be present inside the crater, which have been masked by the stronger variability of saturated spectra. On the other hand, we have not masked the bad channels in the classification procedure, because this would have compromised recognition of the other classes. The mare-like classes are extensively present also on the plateau and in part of the Aristarchus ejecta. The plateau shows two different spectral units: the former, corresponding to the DMD, is represented by class #4 (cyan) while the latter is the already mentioned class #7. Part of the southward Aristarchus ejecta (described by class #1), shows a red slope in the 0.50–0.60 μm region, medium-high albedo and a weak 1 μm absorption. Class #1 is very similar to class #4 even if the latter has a lower red slope and weaker 1 μm absorption.

6. – Comparison with previous works

The Aristarchus region has been studied spectroscopically by several authors [7-11]. In the following we are interested in the recognition of the mineralogical composition of the spectral units previously identified. To this purpose, we will refer to Lucey *et al.* [7] and Hawke *et al.* [9] which have determined the composition of some areas present in the Aristarchus region. Other investigators [8, 10, 11], by using the high-spatial-resolution images of the UVVIS Clementine camera, have outlined with high spatial detail, the distribution of spectral units present in the Aristarchus region. In their studies, Lucey and Hawke have sampled small areas distributed onto the region covered by our image. We have assumed that the mineral assemblages found by them in these restricted regions, are also representative of the composition of larger units shown in fig. 4b). The conclusion of this comparison is shown in last column of table II. The classification map shows that the mare component is widespread on the plateau [10, 11] and in the Aristarchus ejecta. These basalts are at least of two types, respectively, a high TiO_2 content (class #3) and a medium TiO_2 content (class #7) component. The southward ejecta blanket (class #1)

could be dominated by mare assemblages, even if a strong spectral similarity with the DMD present on the plateau exists. The relatively high albedo of this unit and the position of the band shifted toward longer wavelengths could be an indication of olivine. This hypothesis is supported by the detection of olivine in the southern rim crest of Aristarchus made by Hawke *et al.* [9].

7. – Conclusions

The data presented here provide new insights concerning the distribution of different mineralogic units across the Aristarchus region. Even if the spectral region from 1.1–2.5 μm (diagnostic for recognition of different mafic minerals) is not covered, the study of the albedo, the 0.9–1.1 μm band and UVVIS slope maps gives quantitative information about the spatial distribution of mafic minerals through the lunar surface. Principal-component analysis applied to the Aristarchus image cube has allowed to show all the spectral variability of this region while the spectral clustering has produced a map of the zones having similar spectral behavior. The composition of these spectral units has been correlated with the results reported by Lucey *et al.* [7] and Hawke *et al.* [9]. Material of mare composition appears to be widespread on the plateau and in part of the Aristarchus ejecta. The southwest ejecta of Aristarchus exhibit spectral characteristics similar to the DMD present on the plateau but present higher albedo. Their composition could be dominated by olivine.

* * *

We are particularly grateful to the support staff and telescope operators of the Sierra Nevada Observatory. Without their help the observations described in the paper would not have been possible. We specially thank Dr. J. L. MORENO and Dr. J. RODRIGUEZ of the Institute of Astrophysics of Andalucia for their continuous assistance. Funding were provided by ASI and CSIC grants.

REFERENCES

[1] HEAD J. W., PIETERS C., MCCORD T., ADAMS J. and ZISK S., *Definition and detailed characterization of lunar surface units using remote observations, Icarus*, **33** (1978) 145-172.
[2] MCCORD T. B., CLARK R. N., HAWKE B. R., MCFADDEN L. A. and OWENSBY P. D., *Moon: near-infrared spectral reflectance, a first good look, J. Geophys. Res.*, **86** (1981) 10883.
[3] ADAMS J. B., *Visible and near-infrared diffuse reflectance spectra of pyroxenes as applied to remote sensing of solid objects in the solar system, J. Geophys. Res.*, **79** (1974) 4829-4836.
[4] PIETERS C. M., *Mare basalt types on the front side of the Moon: A summary of spectral reflectance data, Proc. Lunar Planet. Sci. Conf., 9th* (1978) 2825-2849.
[5] ZISK S. H., HODGES C. A., MOORE H. J., SHORTHILL R. W., THOMPSON T. W., WHITAKER, E. A. and WILHELMS D. E., *The Aristarchus-Harbinger region of the Moon: Surface geology and history from recent remote sensing observations, Moon*, **17** (1977) 59-99.
[6] SHORTHILL R. W. and SAARI J. W., *Non-uniform cooling of the eclipsed Moon: A list of thirty prominent anomalies, Science*, **50** (1965) 210-212.
[7] LUCEY P. G., HAWKE B. R., PIETERS C. M., HEAD J. W. and MCCORD T. B., *A compositional study of the Aristarchus region of the Moon using near infrared reflectance spectroscopy, J. Geophys. Res.*, **91** (1986) 344-354.
[8] MCEWEN A. S., ROBINSON M. S., ELIASON E. M., LUCEY P. G., DUXBURY T. C. and SPUDIS P. D., *Clementine observations of the Aristarchus region of the Moon, Science*, **266** (1994) 1858-1862.

[9] HAWKE B. R., PETERSON C. A., COOMBS C. R., LUCEY P. G., SMITH G. A. and TAYLOR G. J., *Remote sensing studies of the Aristarchus region of the Moon* (abstract) *Lunar Planet Sci. XXVI*, **26** (1995) 559-560.

[10] PINET P. C., MARTIN P., COSTARD F., CHEVREL S., BELLAGH F. and BLAMONT J., *Aristarchus plateau spectral mapping from Clementine and telescopic high resolution spectro-imaging data* (abstract), *Lunar Planet. Sci. Conf. XXVI*, (1995) 893-894.

[11] PINET P. C., MARTIN P.: COSTARD F., CHEVREL S., DAYDOU Y. and JOHNSON P. E., *Aristarchus Plateau: Clementine spectro-imaging and geological inferences* (abstract), *Lunar Planet. Sci. Conf. XXVII*, (1996) 1037-1038.

[12] BELLUCCI G., FORMISANO V. and PINORI S., *Imaging spectroscopy of the Moon: Data reduction - Analysis techniques and compositional variability of the Mare Serenitatis-Tranquillitatis region, Planet. Space Sci.* **46** (1998) 377-390.

[13] MCCORD T. B., *Color differences on the lunar surface*, PhD Dissertation, California Institute of Technology, Pasadena, 1968.

[14] PIETERS C. M., *Composition of the lunar highland crust from near-infrared reflectance spectroscopy, Rev. Geophys.*, **20** (1986) 557-578.

[15] CLARK R. and N. ROUSH T. L., *Reflectance spectroscopy: Quantitative analysis techniques for remote sensing applications, J. Geophys. Res.*, **89** (1984) 6329-6340.

[16] MCCORD T. B., CHARETTE M. P., JOHNSON T. V., LEBOFSKY L. A., PIETERS C. M. and ADAMS J. B., *Lunar spectral types, J. Geophys. Res.*, **77** (1972) 1349-1359.

[17] PIETERS C. M., HEAD J. W., SUNSHINE J. M., FISHER E. M., MURCHIE S. L., BELTON M., MCEWEN A., GADDIS L., GREELEY R., NEUKUM G., JAUMANN R. and HOFFMANN H., *Crustal diversity of the Moon: Compositional analyses of Galileo solid state imaging data, J. Geophys. Res.*, **98** (1993) 17127-17148.

[18] DAVIS J. C., *Statistics and Data Analyisis*, in *Geology* (Wiley, New York) 1986.

[19] JAUMANN R., KAMP L. and NEUKUM G., *Spectrophotometric analysis of lunar surface material: a new technique for the quantitative determination of geochemical components* (abstract), *Lunar Planet. Sci. XIX*, (1988) 551-552.

[20] JAUMANN R., *Spectral-chemical analysis of lunar surface materials, J. Geophys. Res.* **96**, (1991) 22793.

[21] ERARD S., BIBRING J. P., MUSTARD J., FORNI O., HEAD J. W., HUTREZ S., LANGEVIN Y., PIETERS C. M., ROSENQVIST J. and SOTIN C., *Spatial variation in composition of the Vallis Marineris and Isidis Planitia Regions of Mars derived from ISM data, Proc. Lunar Planet. Sci. Conf.*, **21** (1991) 437.

[22] CHEVREL S. D., PINET P. C., HEAD J. W. and BELLAGH F., *UV-VIS-NIR spectral classification in the Gruithuisen domes region* (abstract), *Lunar Planet. Sci. XXVI*, (1995) 241-242.

[23] KRUSE F. A., LEFKOF A. B., BOARDMAN J. W., HEIDEBRECHT K. B., SHAPIRO A. T., BARLOON J. P. and GOETZ A. F. H., *The spectral image processing system (SIPS) - Interactive visualization and analysis of imaging spectrometer data, Remote Sensing Environ.*, **44** (1993) 145-163.

[24] YUHAS R. H. and GOETZ A. F. H., *Comparison of Airborne (AVIRIS) and spaceborne (TM) imagery data for discrimination among semi-arid landscape endmembers, Proceedings of the Ninth Thematic Conference on Geologic Remote Sensing* (Environmental Research Institute of Michigan, Ann Arbor, Mich.) 1993, pp. 503-511.

[25] BELLUCCI G. and FORMISANO V., *Regional mapping of planetary surfaces with imaging spectroscopy, Planet. Space Sci.*, **45** (1998) 1371-1381.